

Supplementary Information

One-step Micromolding of Complex 3D Microchambers for Single-Cell Analysis

Hiroaki SUZUKI, Kenta MITSUNO, Katsuyuki SHIROGUCHI, Mamiko TSUGANE, Taiji OKANO, Tetsuji DOHI, Tomoaki TSUJI

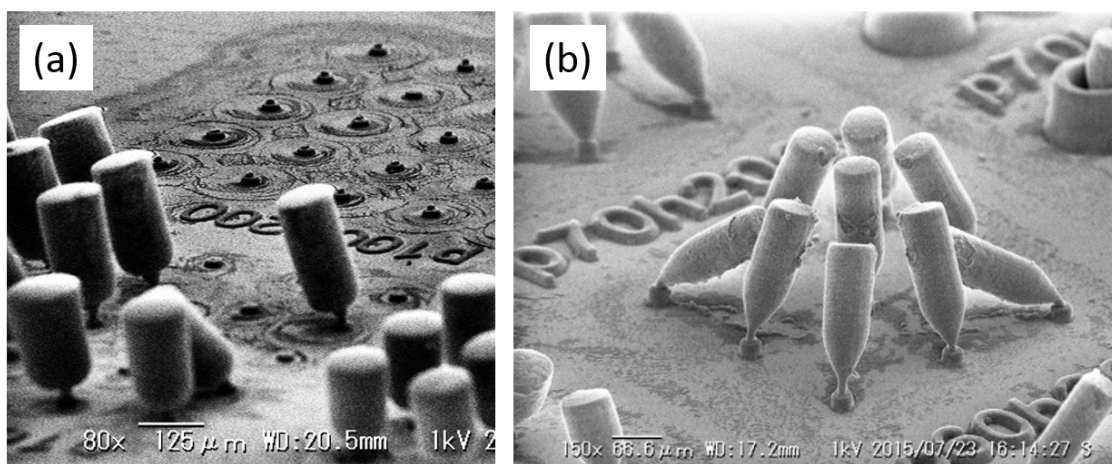


Figure S1. (a) Example of the tilted (down left) and broken (upper right) structures after washing and drying. (b) Example of tilted structures due to the surface tension of solvent during the drying process.

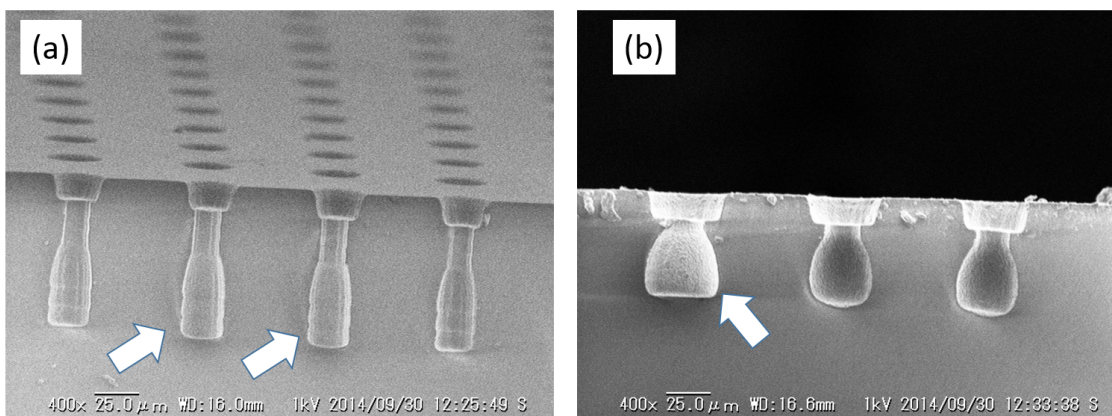


Figure S2. Broken part of the mold which was left in the slab of PDMS (indicated by arrows). This phenomenon occurred when PDMS resin was directly casted over the epoxy mold with no surface treatment.

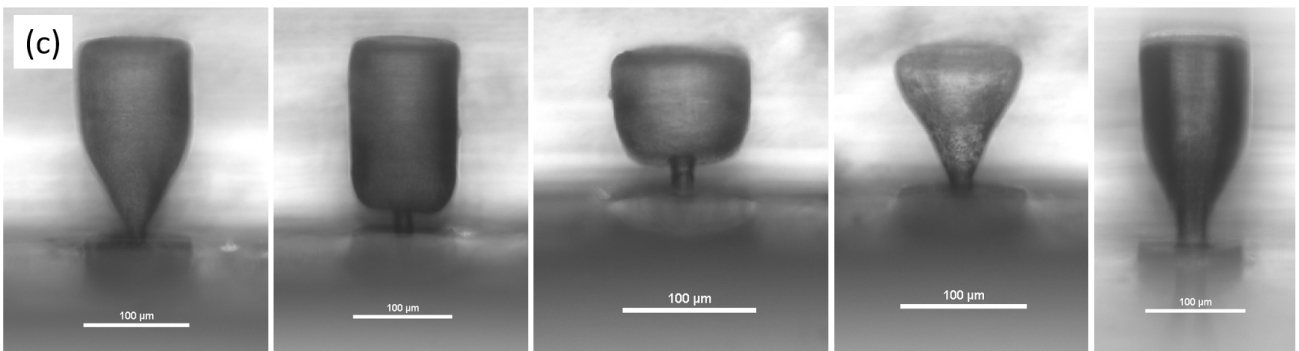
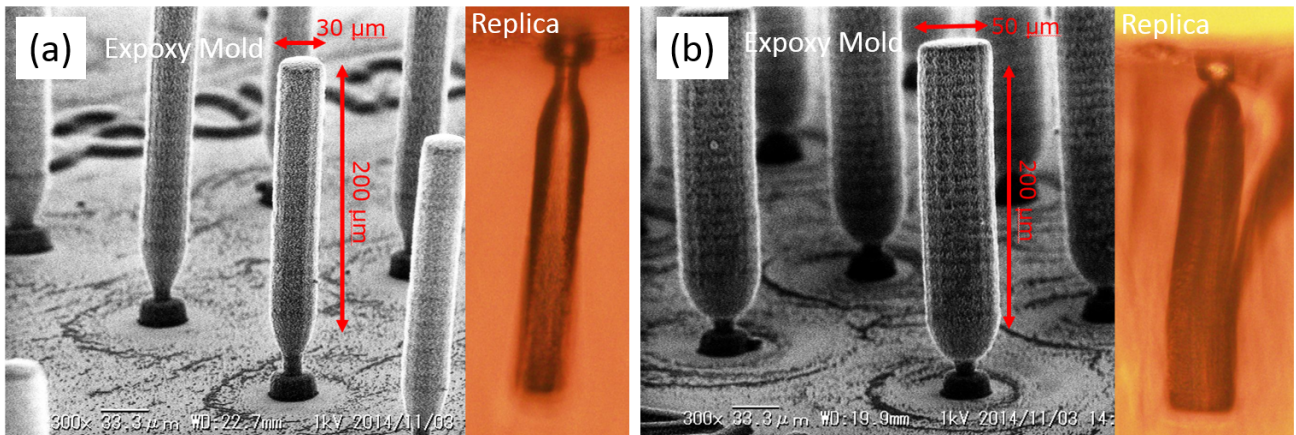


Figure S3 (a, b) Other examples of the mold and corresponding replica. (c) Examples of PDMS replica. Especially for large scale pillars with large separation, it was difficult to cut the PDMS slab at the exact location of axes to obtain SEM images similar to Fig. 2(d) in the main text. In these figures sectional view was obtained by the inverted microscope with the transmitted light. Reservoir or cavity part seems blurred due to the uneven cutting planes.

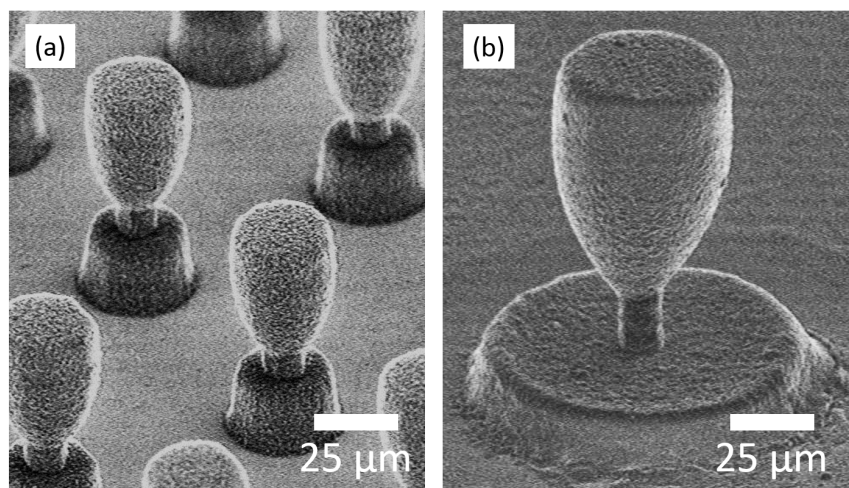
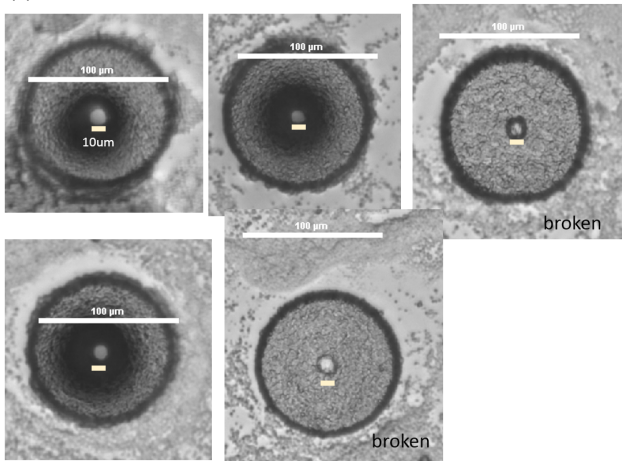
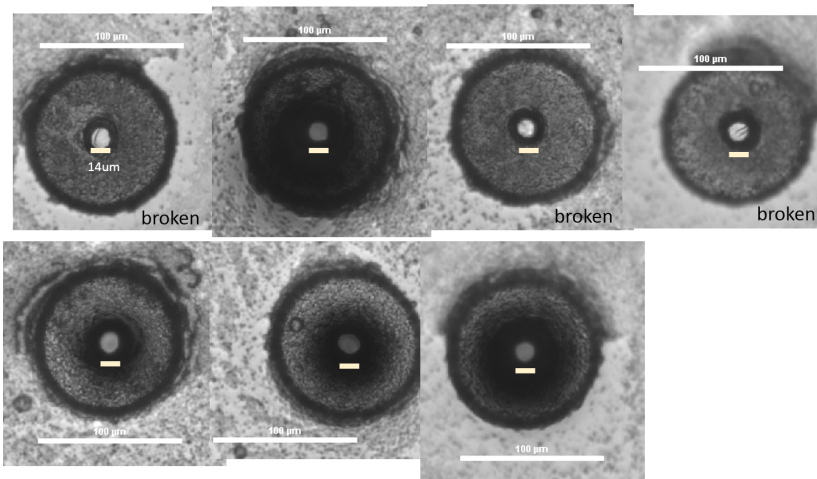


Figure S4 Close-up view of the surface of the mold. (a) Before and (b) after parylene deposition.

(a) Neck diameter 10um



(b) Neck diameter 14um



(c) Neck diameter 20um

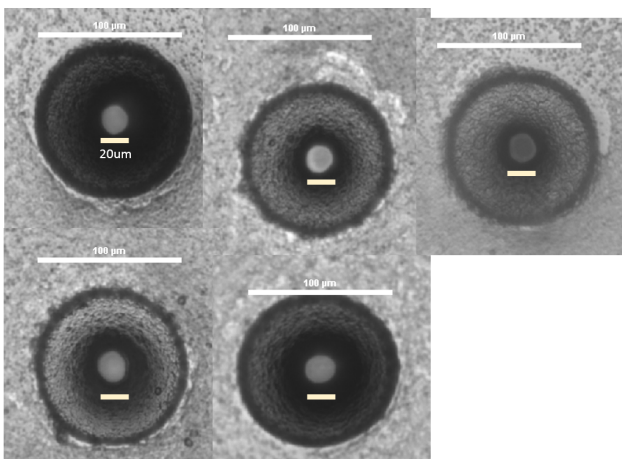


Figure S5. Randomly selected images of the master mold captured by the inverted microscope. The focal planes are adjusted at the neck. Light yellow bars in images show 10, 14, and 20 mm, respectively in (a), (b), and (c), which is nearly the same as the designed neck diameters.

Axi-symmetric deformation analysis of the demolding of silicone elastomer

(A) Formulation

The parameters used in the axi-symmetric model is depicted in Figure S5(a). The free body diagram (FBD) of a slice of the silicone elastomer is depicted in Fig. S5(b).

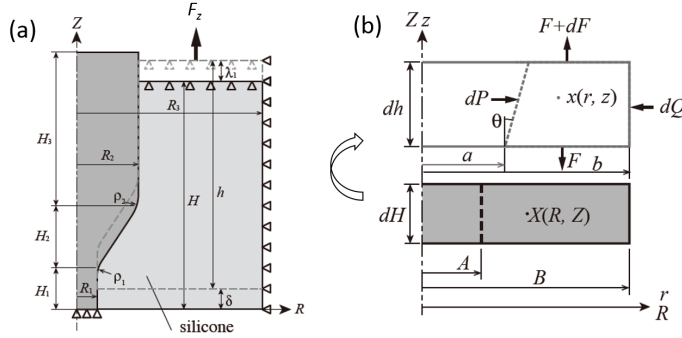


Figure S6 (a) Configuration model of the analysis. (b) FBD of the silicone elastomer with the thickness dH .

Here, the cylindrical coordinates before and after pulling up the silicone elastomer for the vertical displacement δ are denoted as (R, θ, Z) and (r, θ, z) , respectively. In the FBD, deformation is induced by the load dP on the inner cylindrical surface of the elastomer, which expands this surface from A to a in the radial direction. Accordingly, the initial thickness of the slice dH increases to dh (due to the incompressibility), and an arbitrary point in the silicone $X(R, Z)$ moves to $x(r, z)$. The displacement of the upper plane in z direction is assumed to be uniform. The main stretches in R, θ, Z directions are denoted as $\lambda_1, \lambda_2, \lambda_3$, respectively, which are uniform in θ direction. The load on the outer plane is denoted as dQ . The load in Z direction exerted on the upper and lower planes are denoted as F and $F+dF$, respectively. The friction between the epoxy mold and the elastomer is neglected.

At equilibrium, the increment of the load between the upper and the lower plane is related to the radial load dP ,

$$dF = dP \tan \theta, \quad (S1)$$

where θ is the angle between the reverse taper face and the Z axis. The energy density function is denoted as

$$W(\lambda_1, \lambda_2, \lambda_3) = \frac{\mu}{2} (\lambda_1^2 + \lambda_2^2 + \lambda_3^2 - 3). \quad (S2)$$

The stress (conventional stress) is written as

$$t_1^{(1)} = \frac{\partial^2 W}{\partial \lambda_1}, t_2^{(1)} = \frac{\partial^2 W}{\partial \lambda_2}, t_3^{(1)} = \frac{\partial^2 W}{\partial \lambda_3}. \quad (S3)$$

From the assumption that PDMS is incompressible, the relation $\lambda_1 \lambda_2 \lambda_3 = 1$ holds. By rewriting $\lambda_2 = \lambda (= r/R)$, $\lambda_3 = \lambda_z$ (constant), and $\lambda_1 = \lambda^{-1} \lambda_z^{-1}$, we obtain the Neo-Hookean energy function with two parameters

$$\begin{aligned} W(\lambda_1, \lambda_2, \lambda_3) &= \hat{W}(\lambda, \lambda_z) \\ &= \frac{\mu}{2} (\lambda^{-2} \lambda_z^{-2} + \lambda^2 + \lambda_z^2 - 3) \end{aligned} \quad (S4)$$

At equilibrium, we obtain dF in terms of main stretches at inner and outer radial surfaces λ_a and λ_b after integrating the axial stress $t_3^{(1)}$ over the section

$$\left(\frac{dF}{2\pi\mu} \right) = \lambda_a A \left[-\frac{2\lambda_b^{-1}\lambda_z^2}{(B^2 - A^2)} \left(\frac{F}{2\pi\mu} \right) + \left\{ \lambda_z^3 - \frac{1}{2} - \frac{\lambda_z^{-1}}{2} (1 + \lambda_a^{-2} - \lambda_b^{-2}) + \frac{B^2}{(B^2 - A^2)} \ln \frac{\lambda_a}{\lambda_b} \right\} \tan \theta dH \right], \quad (S5)$$

where $\lambda_b = 1$ assuming that the radial position of the outer surface is unchanged. λ_a is derived as a function of δ . The load F_z is calculated by integrating eq. (S5) over the range $0 < z < H$.

The result of the calculation of eq. (S5) using the experimental scales ($R_1 = 5 \mu\text{m}$, $R_3 = 90 \mu\text{m}$, $H_1 = 10 \mu\text{m}$, $H_2 = 40 \mu\text{m}$, $H_3 = 50 \mu\text{m}$) for various R_2 is plotted in Figure S7. The present analytical formulation is able to predict the maximum pulling force within the 10% error compared to the FEM analysis.

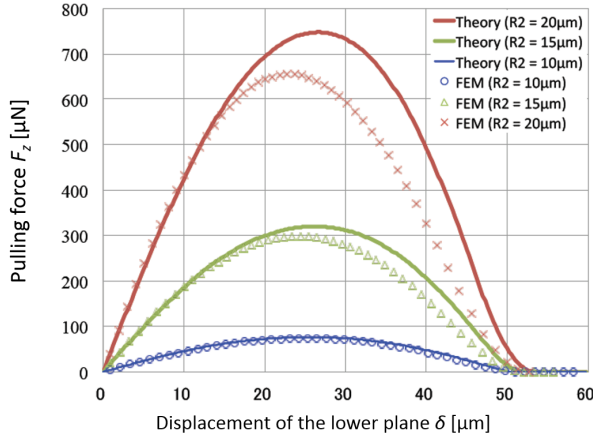


Figure S7. Result of the calculation of F_z . Result of the FEM analysis is also plotted for comparison.

(B) Simplified Model

In the simplified analysis (eq. (1) in the main text), we further made assumption that F_z reaches maximum when the narrowest part at the neck was stretched to the maximum radius of the cylinder, i.e., $\lambda_a = R_1/R_2$. Note that in this case $F = 0$ and $dF = F_z$ in Figure S6. By substituting the following relations

$A = R_1$, $a = R_2$, $\lambda_b = 1$, $\lambda_z = 1$, $B^2/(B^2 - A^2) = 1$, $\tan \theta = (R_2 - R_1)/H_2$, eq. (S5) is re-written as

$$\begin{aligned} F_z &= 2\pi\mu \cdot \lambda_a A \left\{ 1 - \frac{1}{2} - \frac{1}{2} (1 + \lambda_a^{-2} - 1) + \ln \frac{\lambda_a}{1} \right\} \tan \theta dH \\ &= 2\pi\mu \cdot \frac{R_2 H_1 (R_2 - R_1)}{H_2} \left\{ \frac{R_2^2 - R_1^2}{2R_2^2} + \ln \left(\frac{R_2}{R_1} \right) \right\} \end{aligned} \quad (S6)$$

Using $2R_1 = d$ and $2R_2 = D$, eq. (S7) is expressed as eq. (1) in the main text.

(C) Modified simple model

In the model (B), we assumed $B \gg A$ and $\lambda_z = 1$ (no vertical stretch). Here we take the finite scale of the PDMS in radial direction, R_3 , into account. This situation corresponds to the placement of a large number of posts in array format, where the separation between posts is $X = 2R_3$. By substituting the following relations

$$A = R_1, a = R_2, \lambda_a = R_1/R_2, \lambda_b = 1, \lambda_z = \frac{R_3^2 - R_1^2}{R_2^2 - R_1^2}, \frac{B^2}{B^2 - A^2} = \frac{R_3^2}{R_3^2 - R_1^2}, \tan\theta = (R_2 - R_1)/H_2,$$

eq. (S5) is re-written as

$$\begin{aligned} \left(\frac{dF}{2\pi\mu} \right) &= \frac{R_2}{R_1} R_1 \left[0 + \left\{ \lambda_z^3 - \frac{1}{2} - \frac{1}{2} \lambda_z^{-1} \lambda_a^{-2} \right\} + \left(\frac{B^2}{B^2 - A^2} \right) \ln \frac{\lambda_a}{1} \right] \frac{R_2 - R_1}{H_2} H_1 \\ &= R_2 \left[\left\{ \lambda_z^3 - \frac{1}{2} - \frac{1}{2} \lambda_z^{-1} \lambda_a^{-2} \right\} + \left(\frac{R_3^2}{R_3^2 - R_1^2} \right) \ln \lambda_a \right] (R_2 - R_1) \frac{H_1}{H_2} \end{aligned} \quad (S8)$$

In this case, the mean stress at the narrowest neck part of the mold (parlylene was not considered for simplicity) is

$$\sigma = 2\mu \frac{DH_1(D-d)}{d^2 H_2} \left[\left\{ \lambda_z^3 - \frac{1}{2} - \frac{1}{2} \lambda_z^{-1} \left(\frac{d}{D} \right)^2 \right\} + \left(\frac{4R_3^2}{4R_3^2 - d^2} \right) \ln \left(\frac{d}{D} \right) \right], \quad (S9)$$

where

$$\lambda_z = \frac{4R_3^2 - d^2}{4R_3^2 - D^2}. \quad (S10)$$

The result of eq. (S9) for $d = 10 \mu\text{m}$ is plotted in Figure S8. Because of the constraint in the radial strain and stretching in z direction, $\sigma (F_z)$ slightly increases, but the difference becomes observable only when the inter-pillar distance X is similar to the reservoir diameter D . In our experiment, X was typically 200 or 300 μm .

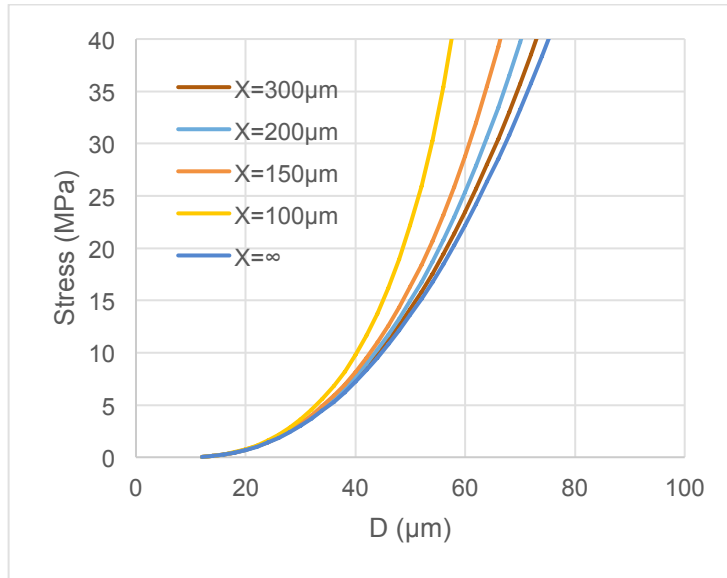


Figure S8. Stress exerted on the neck for $d = 10 \mu\text{m}$ estimated with eqs. (S9) and (S10). $X=\infty$ corresponds to the simplified model (B).

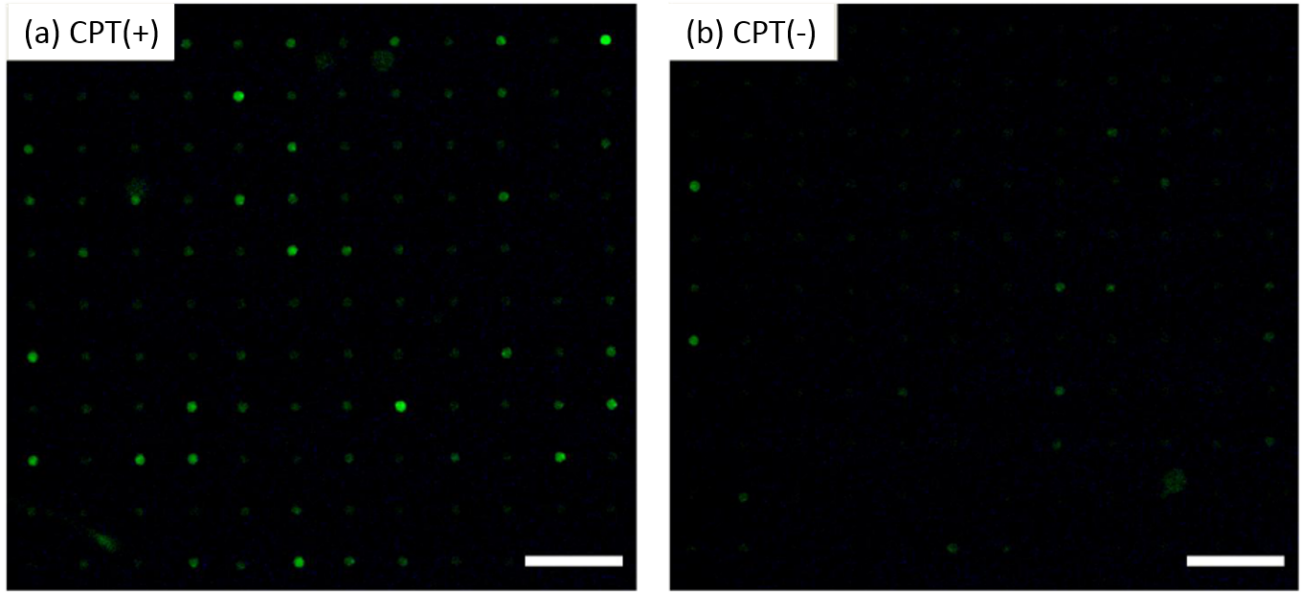


Figure S9. Fluorescence image of the single-cell apoptosis assay. (a) With camptothecin (CPT) treatment. (b) Without CPT treatment, the signal indicating apoptosis is extremely low.